



Improvement of Optical Properties of Functionalized Polyvinyl Alcohol-Zinc Oxide Hybrid Nanocomposites for Wide UV Optoelectronic Applications

Alaa M. Abd-Elnaiem¹ · M. Rashad^{1,2} · T. A. Hanafy^{2,3} · N. M. Shaalan^{4,5}

Received: 6 February 2023 / Accepted: 14 March 2023 / Published online: 12 May 2023
© The Author(s) 2023

Abstract

The functionalized polyvinyl alcohol (PVA) based nanocomposites thick films of 80 μm containing 1–3 wt% zinc oxide (ZnO) nanoparticles (NPs) were studied. X-ray diffraction (XRD), Fourier transform infrared spectroscopy (FTIR), and Raman spectroscopy were utilized for studying the structural parameters and formed chemical bonds of the synthesized PVA-ZnO films. In addition, extensive characterization has been done on their linear and nonlinear optical properties. The structural analysis of the PVA-ZnO nanocomposites revealed the formation of a wurtzite hexagonal ZnO phase embedded inside the monoclinic PVA phase. The interaction between Zn–O, and functional groups of the PVA as well as the molecular vibration exhibited in the PVA-ZnO nanocomposites were confirmed by the Raman and FTIR spectroscopy and revealed that the PVA-ZnO is a hybrid nanocomposite. The incorporated ZnO NPs ratios slightly affect the PVA films' structure, meanwhile, exhibited a detectable change in the linear/nonlinear optical properties of PVA. For example, as ZnO concentration increased from 1 wt% to 3 wt%, the direct/indirect optical band gap of PVA slightly decreased from 5.1/4.93 eV to 4.45/4.89 eV, respectively. Other optical characteristics, such as optical conductivity, dielectric constants, absorption coefficient, refractive index, etc., were evaluated. All observed optical properties versus energy/wavelength display a distinct pulse at 1.4 eV/850 nm which corresponds to the difference between the direct and indirect optical band gaps. It is expected that PVA-ZnO hybrid nanocomposites have become appropriate for implementation in numerous electronic applications due to their improved optical characteristics.

Keywords PVA · ZnO · Polymer functionalization · Oxides · Optical properties

1 Introduction

A polar organic polymer such as polyvinyl alcohol (PVA) has received a lot of interest in recent years due to its highly transparent, mechanical flexibility, affordable, non-toxic, high biocompatibility, and good storage properties as well as strong chemical and thermal stabilities [1–3]. The new characteristics of PVA-based materials have made them appropriate for a range of applications especially optoelectronic technology [4]. One might modify the behavior of optoelectronic devices by dispersing one or more nanofiller (such as metal oxide, rare earth salt, etc.) inside the PVA matrix [5, 6]. The linear and nonlinear optical characteristics of PVA have changed as the result of modifications in the internal structure of the material, which led to the formation of complex interfaces or supermolecules inside this polymeric material [7]. It is well known that non-covalent bonds like hydrogen and coordination bonds play a key

✉ Alaa M. Abd-Elnaiem
abd-elnaiem@aun.edu.eg

✉ M. Rashad
m.ahmad@ut.edu.sa

¹ Physics Department, Faculty of Science, Assiut University, Assiut 71516, Egypt

² Department of Physics, Nanotechnology Research Laboratory, Faculty of Science, University of Tabuk, Tabuk, Saudi Arabia

³ Department of Physics, Faculty of Science, Fayoum University, El Fayoum 63514, Egypt

⁴ Department of Physics, College of Science, King Faisal University, P.O. Box 400, Al-Ahsa 31982, Saudi Arabia

⁵ Energy and Sensing Laboratory, Physics Department, Faculty of Science, Assiut University, Assiut 71516, Egypt

role in PVA's super-molecular structural design [1]. PVA is regarded as a fixable insulator since it has a wide band gap and may be modified to have a greater or lower band gap for use in various optical applications [7]. The significance of the produced composites in optoelectronic applications is highlighted by the small dimensions of the disseminated nano-filler and the broad interacted surface with the polymer [8]. The key rationale for selecting this type of nanoparticle is that they have a large optical band gap. Therefore, it is necessary to examine the impact of the interpolation process between the nano-filler particles and polymer bases to study their physical aspects in addition to the optical parameters [9].

It is essential to develop polymers that are suitable for a wide range of applications by incorporating nanoparticles or modifying them with additional treatment. For example, the doping polymers like poly(aniline-co-pyrrole) with metal oxides like ZnO nanoparticles to form poly (aniline-co-pyrrole)-ZnO nanocomposites increases their applicability as shielding for protecting the eyes and optical equipment from high-intensity lasers [10]. Similarly, doping poly (aniline-co-ortho phenylenediamine) polymers with TiO₂ nanoparticles enhances their refractive index and qualifies them for nonlinear optical applications [11]. The development of PVA using transition metal oxides could be applied in optoelectronics, catalysis, energy storage, and other fields making them intriguing semiconductors [12]. The electronic (optical and electrical) properties of PVA may be improved and controlled by doping metal and metal oxide nanoparticles such as Ni, Fe, ZnO, multi-walled carbon nanotubes (MWCNTs), etc. [13–16]. The doping PVA by MWCNTs can improve the PVA's electronic characteristics, for instance, the electrical conductivity of PVA-MWCNTs significantly increases with a percolation threshold of roughly 4 wt% MWCNTs [14]. The optical band gap of PVA was significantly reduced from 5.3 eV to 2.3 eV by adding 3.7 wt% Ni or 3 wt% Fe [13, 15]. Falamas et al. have investigated the surface-enhanced fluorescence potential of ZnO nanoparticles and Au-decorated ZnO nanostructures embedded in a PVA matrix [17]. Similarly, the optical properties of synthesized PVA-zinc peroxide (ZnO₂) nanocomposite films with 0.25–3 wt% ZnO₂ were studied [1].

Among the fillers discussed, ZnO is the most widely utilized filler for functionalizing PVA to enhance its physical characteristics and hence improve its optoelectronics performance [18]. Many studies concerning the development, characterization, and applications of PVA-ZnO nanocomposites employing a variety of methodologies have been published in the literature. In the text that follows, we addressed these studies. ZnO nanoparticles (NPs) were selected as the doping components for PVA because they are widely recognized for possessing distinct band gaps of 3.2 eV [19, 20]. The mechanical and optical characteristics of ZnO-PVA

nanocomposites were recently explored using the chemical oxidative polymerization process [21]. The developed PVA-ZnO nanocomposites may be employed for a proton exchange membrane separator in a single-chambered microbial fuel cell, food packaging, dyes degradation, air filters, photodiodes, and solar cell covering [7, 22–27]. The PVA-ZnO nanocomposites may be synthesized using several techniques, including the sol–gel method, hydrothermal method, electrospinning method, coating method, solution casting technique, and ball mill machine [7, 16, 26, 27]. The optical band gap of pure PVA is typically reported to be approximately 5.3 eV and may be decreased to less than 3 eV by doping ZnO [16]. Methylene blue is effectively discolored by adsorption degradation using the freeze–thaw loading of ZnO nanoparticles to PVA/cellulose nanofibril aerogel [22]. The structural parameters and optical band gap of the PVA-*x* ZnO ($5 \leq x \text{ (mol\%)} \leq 20$) prepared by the solution casting technique were determined [16]. The produced PVA-ZnO films exhibit a redshift in comparison to pure ZnO, even though the ZnO ratio very marginally affects the structural characteristics. Additionally, the intensity of the blue emission in the photoluminescence (470 nm), which fluctuates with the ratio of ZnO, reaches its maximum at 10 mol% of ZnO. The structural and optical properties of PVA-*x* ZnO ($0 \leq x \text{ (wt\%)} \leq 3$) prepared using the sol–gel method were studied [27]. The dielectric constant and response of the PVA-ZnO nanocomposite films were evaluated [28–30]. The antibacterial inhibitory efficacy of ZnO/PVA was observed to rise with an increase in the ZnO ratio in PVA-based nanocomposites, particularly PVA-ZnO, which is typically utilized for food backing [23].

The preparation technique has an impact on the structural characteristics of PVA polymer, which are similar to those of other materials. Additionally, the optical absorbance and subsequently all other optical parameters are strongly impacted by the nanocomposite films' thickness. Additionally, the kind and ratio of metal oxide doping greatly influence the physical characteristics, particularly the optical parameters. Only a few optical characteristics, such as the refractive index, extension coefficient, optical band gap, and certain dispersion parameters of various ZnO thicknesses and ratios, were studied in the literature when it related to the optical properties of PVA-ZnO nanocomposites [16, 23, 27].

It is well understood that the casting procedure is mainly dependent on dissolving both the host and the additional elements in the same solvent whenever feasible. Moreover, the suitable solvent for PVA is distilled water, whereas metal oxides do not dissolve in water. As a result, utilizing this approach to synthesize PVA/ZnO nanocomposites is extremely challenging, especially at greater concentrations of ZnO NPs. A suspended solution of ZnO with water may be produced at tiny concentrations of ZnO ranging from 1

to 3 wt%. As a result, the casting process may be employed in this scenario under specific circumstances such as the stirring time and temperature, which are considered in this article. Therefore, the present study intends to enhance the structural and linear/nonlinear optical properties of the PVA polymer and make them more applicable by incorporating different concentrations (1, 2, or 3 wt%) of ZnO NPs. In addition, a systemic evaluation of the linear and nonlinear optical properties of 80 μm thick PVA-ZnO nanocomposites is performed. A variety of methods, including XRD, FTIR, Raman spectroscopy, and double-beam spectrophotometer, were used to complete the study. The results demonstrated that PVA-ZnO hybrid nanocomposites may be used for optoelectronic applications that required broadband gap energy.

2 Experimental Details

2.1 Sample Preparations

A solvent casting technique was used to prepare PVA- x wt% ZnO nanocomposite films where $x=1, 2,$ and 3 . More details about the preparation of the PVA-based nanocomposite samples using the solvent casting technique are available elsewhere [5]. The PVA solution, which serves as the host material, was initially made by thoroughly combining 2 g of pure PVA powder (average molecular weight = 17000 g/mol) with 100 ml of deionized water at 353 K and then was stirred using a magnetic stirrer for around 1 h. After that, 20 ml of the diluted PVA solution was stirred continuously for 6 h at 50 °C with 1, 2, or 3 wt% of specifically made ZnO NPs (with a purity of 99.9% and particle size of 30 nm). The PVA/ZnO mixes were then placed in a petri dish and allowed to dry at 40 °C for 6 days. The thickness of the prepared PVA-ZnO nanocomposite was estimated to be about 80 μm .

2.2 Sample Characterization

The crystal structure of the PVA-ZnO nanocomposite films as they had been formed was evaluated using an XRD model a Shimadzu XD-3A diffractometer. The monochromatic Cu- K_{α} source was used to record the XRD spectra in the range of 2θ from 4° to 80° with a step size of 0.06°/s. FTIR spectra were recorded using a Bruker Vector 22 in the wavenumber range from 400 to 4000 cm^{-1} to describe the molecular structure of the PVA-ZnO nanocomposite films. Raman spectrometer model Lab-RAM HR800, Horiba, France, coupled to a multichannel charge-coupled detector was used to study the chemical bonding and intramolecular bonds of the PVA-ZnO nanocomposites. The Raman spectra were captured in the spectrum range of 100–2000 cm^{-1} using a He-Ne laser ($\lambda = 633$ nm, output power = 20 mW,

and spectral resolution = 0.8 cm^{-1}). The transmittance $T(\lambda)$ and reflectance $R(\lambda)$ were measured using a double beam spectrophotometer model LAMBDA™ 750 UV/Vis/NIR at room temperature in the wavelength range of 190–2000 nm.

3 Results and Discussion

3.1 Structural Analysis

The concentrations of 1, 2, and 3 wt% ZnO NPs were chosen as PVA filler materials since they are suitable and effective for PVA doping operation. A PVA sample with 1, 2, and 3 wt% metal oxide components such as ZnO NPs makes an excellent flexible film. Moreover, utilizing these ZnO concentrations in PVA ensures that the ZnO particles have nano dimensions inside the PVA framework. By using small amounts of ZnO NPs as an additive, there is little chance of accumulation or cluster formation. Moreover, various works have been published that investigate the effect of metal salts or metal oxide concentration on the optical, electrical, and dielectric properties of PVA [3–5]. Most of these papers imply that metal oxide NP concentrations of 1, 2, 3, 4, or 5 wt% are suitable dopant concentrations for various polymers.

Our understanding of the crystal structure, crystallite orientation and crystalline sizes within the material are determined by XRD. Figure 1a displays XRD patterns of PVA containing 1, 2, and 3 wt% of ZnO NPs. There are few diffraction peaks were observed for PVA-ZnO containing 1 wt% ZnO belonging to the PVA at 2θ equals 19.06, 22.77, 25.23, 52.92, and 72.19° corresponding to the Miller indices of (110), (200), (104), (400), and (410), respectively. The XRD investigation indicated that the PVA has a monoclinic crystal structure, which is consistent with Ref. [31]. Additional diffraction peaks were observed for a higher concentration of ZnO at 2θ equals 46.238° corresponding to the Miller indices of (204). The diffraction peak at 2θ equals 22.77° was disappeared for ZnO concentrations of 2 and 3 wt%. Such a diffraction pattern has been correlated with the atactic PVA trans-planar conformation [32]. The PVA's crystalline nature could be attributed to the strong hydrogen bond interactions between its chain molecules [2, 26]. For further increases in the ZnO NPs content above 1 wt%, there are other peaks belonging to the ZnO phase besides the observed peaks to the PVA matrix. The observed peaks belong to the wurtzite hexagonal crystal structure of the ZnO phase according to the JCPDS card no. 36-1451. The observed peaks for the ZnO phase are located at 2θ equals 31.57, 34.25, 36.46, and 62.54° corresponding to the Miller indices of (100), (002), (101), and (103), respectively. As the concentration of ZnO increased the location of the diffraction peaks shifted to lower values and most of the diffraction

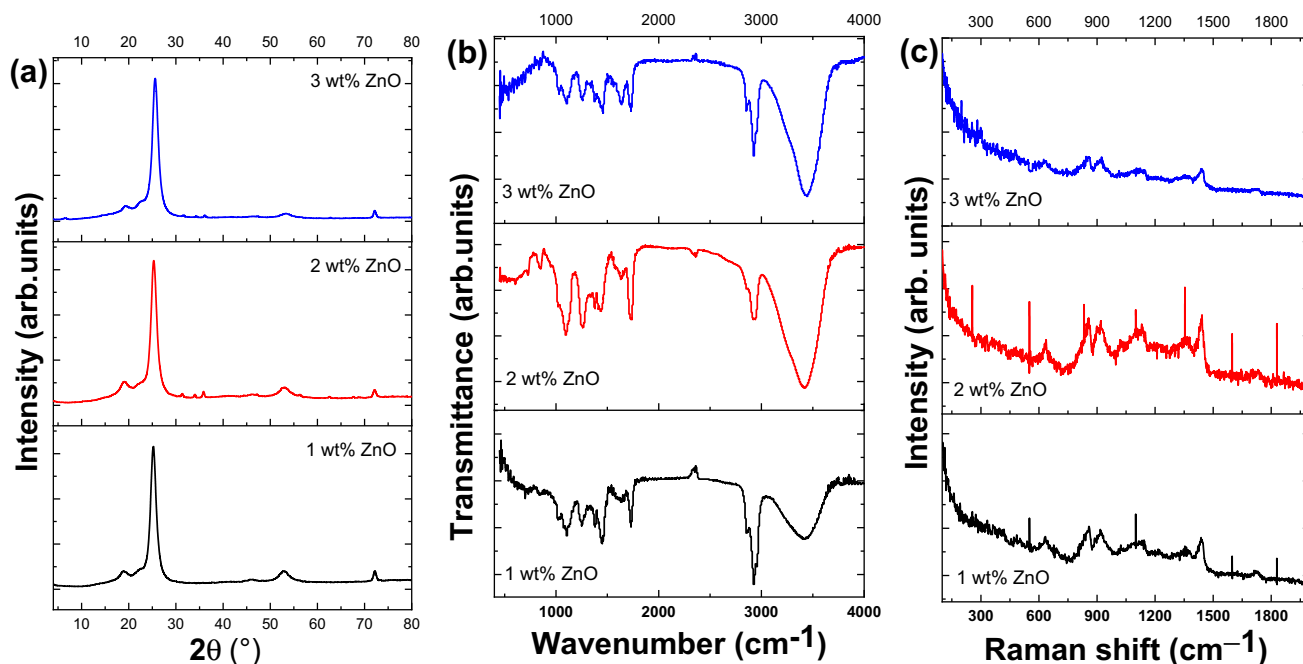


Fig. 1 **a** XRD, **b** FTIR and **c** Raman spectra for as-prepared PVA-*x* wt% ZnO nanocomposite films, where $0 \leq x \leq 3$

peaks belonging to the ZnO phase disappeared. As seen from Fig. 1a, the XRD patterns of PVA-ZnO nanocomposite samples are not drastically changed, and the intensity of the diffraction peaks due to the ZnO phase are very small as their low content in the composites. In general, there is a slight change in the XRD patterns with increasing the ratio of ZnO in the PVA-ZnO nanocomposites. This indicates that PVA is not affected due to the addition of ZnO NPs due to its low concentrations. There are wide and broad peaks at 20.11° that can be seen in the majority of the PVA XRD patterns reported in the literature, however, in this work, the XRD patterns are different. Although the observed diffraction peaks for PVA-ZnO nanocomposites are comparable to those previously noted, the present study's modest ZnO content has significantly reduced their intensity. The decrease in the number of hydrogen bonds that formed between the functional groups of PVA and ZnO nano-molecules is responsible for the decrease in crystallinity. Moreover, the breakage of the crystal phases could be assigned to the decrease of the intermolecular hydrogen bonding between the main chains of PVA-ZnO nanocomposites. Consequently, a decrease in the degree of the crystallinity of PVA-ZnO samples can be expected [33]. Furthermore, it is possible to interpret the PVA-ZnO nanocomposites decreased peak intensity and increased peak broadening as a result of the ZnO NPs capacity to construct a covalent bond with OH of the PVA structure. As a result, it is possible to produce the crosslinking formation between the OH of the PVA and the ZnO NPs.

The average crystallite size (D), microstrain (ϵ), dislocation density (δ), and stacking fault (SF) for PVA-ZnO nanocomposites are estimated using [34–36]: $D = \frac{K\lambda}{\beta \cos(\theta)}$, $\epsilon = \frac{\beta \cos(\theta)}{4}$, $\delta = \frac{1}{D^2}$, and $SF = \frac{2\pi^2}{45\sqrt{\tan(\theta)}}\beta$, respectively, where β is the full width at half maximum (FWHM) of the observed peak in radian, and K is a constant called the shape factor and equal to 0.89. The diffraction peaks, Miller indices, and other structural parameters for PVA, and ZnO phases are summarized in Table 1. The average crystallite size and stacking fault values for the ZnO and PVA phases were increased with the increase of ZnO fraction in the PVA-ZnO nanocomposites. Additionally, as the ZnO concentration in the PVA-ZnO nanocomposites was increased, the average values of the microstrain and dislocation density were reduced.

The small variation in the crystal structure of the PVA-ZnO nanocomposites with the ZnO ratio may be explained by the low concentration of ZnO NPs inside the PVA matrix. The structural characteristics of the ZnO phase alter only marginally as the doping ratio of ZnO NPs increases. Meanwhile, the average crystallite size of the PVA phase grew from 4.05 nm to 8.94 nm when the concentration of ZnO NPs was raised from 1 wt% to 3 wt%, respectively.

A change in the chemical structure and chemical bonds in the polymer/oxides composites is usually analyzed by FTIR spectroscopy. Figure 1b shows FTIR spectra of PVA doped with 1, 2, and 3 wt% ZnO NPs. It is noticed from this figure, a prominent band at 3284 cm^{-1} that is associated with the PVA main chain's OH stretching vibration. It indicates

Table 1 Crystal structure parameters of PVA-*x* wt% ZnO nanocomposites

<i>x</i> (wt%)	2θ (°)	(hkl)	Phase	FWHM (nm)	$SF \times 10^{-2}$	$\overline{SF} \times 10^{-2}$	<i>D</i> (nm)	\overline{D} (nm)	$\epsilon \times 10^{-2}$	$\overline{\epsilon} \times 10^{-2}$	$\delta \times 10^{-3}$ (nm ⁻²)	$\overline{\delta} \times 10^{-3}$ (nm ⁻²)
1	19.06	(110)	PVA	0.055	5.92	3.82	2.799	4.05	8.2	4.65	12.76	7.40
	22.77	(200)		0.043	4.16		3.657		5.3		7.48	
	25.23	(104)		0.027	2.52		5.759		3.0		3.02	
	52.92	(400)		0.043	2.67		3.969		2.1		6.35	
	18.889	(110)		PVA	0.029	3.08	4.31	5.403	3.74	4.3	3.76	3.43
25.320	(104)	0.024	2.21			6.548		2.6		2.33		
46.238	(204)	0.104	7.01			1.588		6.1		39.65		
53.050	(400)	0.057	3.51			3.015		2.8		11.00		
72.317	(410)	0.088	4.52			2.143		3.0		21.78		
3	31.566	(100)	ZnO	0.120	9.88	8.43	1.324	1.60	10.6	8.85	57.09	43.90
	34.247	(002)		0.088	6.99		1.805		7.1		30.70	
	19.142	(110)		0.021	2.21	4.87	7.475	8.94	3.1	2.06	1.79	4.15
	53.380	(400)		0.055	9.02		3.120		2.7		10.27	
	72.172	(410)		0.012	3.38		16.243		0.40		0.38	
30.244	(100)	ZnO	0.093	18.50	18.5	1.694	1.69	8.6	8.6	34.85	34.85	

that a significant number of free OH groups are present in the polymer matrix [8]. The position of this band for PVA-ZnO nanocomposites was shifted to higher frequencies and undergoes an increase in both the transmission value and its broad. This demonstrates ZnO molecules interact with the functional groups of the PVA structure [28]. This suggests that a variety of OH groups and bound OH stretching vibrations are present [37]. So, the complexes formed between ZnO and PVA can be anticipated due to weak interaction of either single or doubly ionized states of Zn (Zn^{-1} and Zn^{-2}) with the functional OH groups of PVA. The CH bond's symmetric and asymmetric stretching vibrations are combined by the bands at 2939 and 2912 cm^{-1} , respectively. The peak position of these bands was shifted to higher frequencies at 2926 cm^{-1} and 2941 cm^{-1} for PVA doped with 2 and 3 wt% of ZnO NPs, respectively. This can be attributed to the hydrogen bonding that formed as a result of the interaction between PVA's CH groups and ZnO NPs [38]. The carbonyl groups (C=O) of PVA were detected at 1732 cm^{-1} where the position of this band was shifted to higher frequencies for PVA-ZnO nanocomposites at 1735 cm^{-1} . So, the interaction between ZnO and C=O of PVA molecules plays a significant role in this process. It is reported that the crosslinking formation within the PVA structure is due to the interaction between ZnO NPs and the functional groups of PVA like OH groups [39, 40]. The C–O band of acetyl groups stretching vibrations is observed at different peaks from 1241 cm^{-1} to 1087 cm^{-1} for all PVA-ZnO nanocomposites. Moreover, the band at 440 cm^{-1} for PVA-ZnO nanocomposites is indicative of Zn–O bond which is affected by the ratio of ZnO NPs in the PVA matrix. The peak position of Zn–O is distributed from 470 cm^{-1} to 558 cm^{-1} with the increase of ZnO NPs content within the PVA-ZnO nanocomposites. These observed peaks may be assigned to the interactions between ZnO particles and PVA structure [41, 42]. Accordingly, the components of PVA-ZnO nanocomposites interact significantly.

The various forms of molecular vibration of PVA-ZnO nanocomposites including stretching, bending, scissor, twisting, and wagging motions of various molecular groups, have been investigated using Raman spectroscopy. Raman spectroscopy is a versatile technique for detecting dopant incorporation impurities, defects, and the lattice disorder phases within the host material [43, 44]. Consequently, the interaction of ZnO NPs with PVA as a host material has been investigated using Raman spectroscopy. Figure 1c shows the different modes of vibration of PVA-ZnO nanocomposites. The carbonyl (C=O) stretching caused by both the acetyl group of PVA and ZnO stretching is the most noticeable vibration in samples of PVA-ZnO nanocomposites. The C=O group in PVA is thought to be the cause of the vibration at 1685 cm^{-1} which is observed as a weak peak. The peak height of the C=O band is reduced with

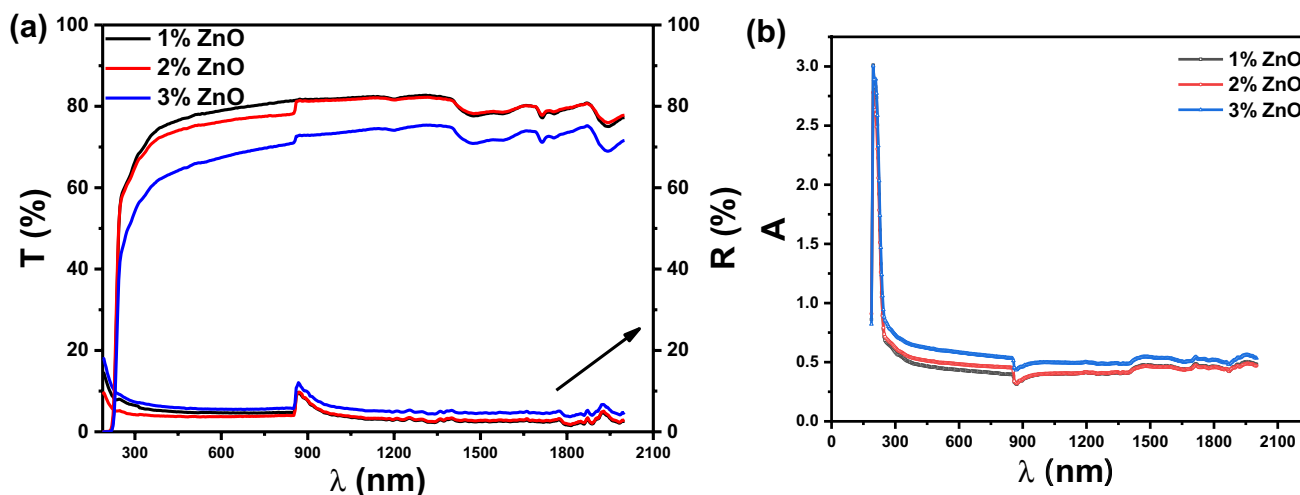


Fig. 2 **a** The transmittance (T), and reflectance (R), and **b** the absorbance (A) as a function of wavelength (λ) for PVA-ZnO nanocomposites

an increase in ZnO concentration. There is some electrical interaction between ZnO NPs and the C=O groups of the PVA structure, as evidenced by the drop in peak height and rise in peak broadness of C=O [12, 45]. The observed peak at 1388 cm^{-1} is assigned to both the C–O stretch and CH_2 scissor. The observed peak at 1330 cm^{-1} corresponds to CH bending in PVA-ZnO samples due to the inter-molecular and intra-molecular interactions. The detected peaks at 828 and 888 cm^{-1} are assigned to C–C chain in the polymer backbone. The peak intensity fluctuation in PVA-ZnO nanocomposites shows a chemical structural modification due to the inter-molecular and intra-molecular interactions between the PVA molecules and ZnO NPs in the polymeric nanocomposites. The two peaks located at 486 and 592 cm^{-1} may be ascribed to the defects of the oxygen atom for ZnO NPs or the broken symmetry induced by the incorporation of ZnO dopants into the PVA structure [46]. Raman spectra analysis shows that PVA-ZnO nanocomposites are hybrid materials with modified properties caused by the charge transfer and the dopant nanomaterials. The ZnO filler affects the degree of crystallinity of the nanocomposite samples and the latter depends on the interaction between the Zn^{2+} , O^{2-} , and the functional OH groups of the PVA.

3.2 Optical Properties

The analysis of transmittance (T) and reflectance (R) of PVA-ZnO nanocomposites was accomplished to explore their optical parameters and constants, then specify their proper applications. The optical properties of PVA before doping with ZnO were studied in detail in our previous work [5]. The transmittance and reflectance of the various PVA-ZnO nanocomposites versus a wide range of wavelengths starting from the ultraviolet to the near-infrared region

(190–2000 nm) are shown in Fig. 2a. The film thickness is $80\text{ }\mu\text{m}$ for various studied PVA-ZnO nanocomposites. It is noticed from Fig. 2a that the transmittance passes two stages depending on the incident wavelength: (1) in the wavelength range 200–260 nm (ultraviolet region), T is remarkably increased with increasing the incident wavelength. (2) for wavelengths higher than 260 nm, T is slightly increased with increasing wavelength and then barely increases to reach a steady value for the remaining part of the investigated wavelength. The PVA-ZnO nanocomposites exhibit a high transmittance for the wavelength above 350 nm and reach 82.7% for PVA-ZnO nanocomposites. Contrary to T, the value of R shows a tendency to decrease with increasing the incident wavelength.

The absorbance (A) of the various PVA-ZnO nanocomposites versus the incident wavelength is shown in Fig. 2b. On the same track of T, A passes two stages depending on the incident wavelength: (1) in the wavelength range 200–280 nm (ultraviolet region) A is sharply decreased with increasing the incident wavelength. (2) For wavelengths higher than 280 nm, the value of A is slightly decreased with increasing wavelength and then barely decreases to reach a steady value for the remaining part of the investigated wavelength. From the calculated data using: $A = \sqrt{\ln\left(\frac{1-R}{T}\right)}$ [13], it turns out that the average absorbance is equal to 0.49, 0.50, and 0.59 for PVA-ZnO nanocomposite containing 1, 2, and 3 wt% ZnO NPs, respectively. The absorbance in the present study is much lower than the absorbance by PVA-ZnO when the ratio of ZnO is greater than 5% and less than 19% [23]. The absorbance of PVA-ZnO nanocomposites displayed behaviors that were comparable to those of pure PVA, although the absorbance's value was markedly increased by the ratio of ZnO to PVA. Additionally, when MWCNTs filler

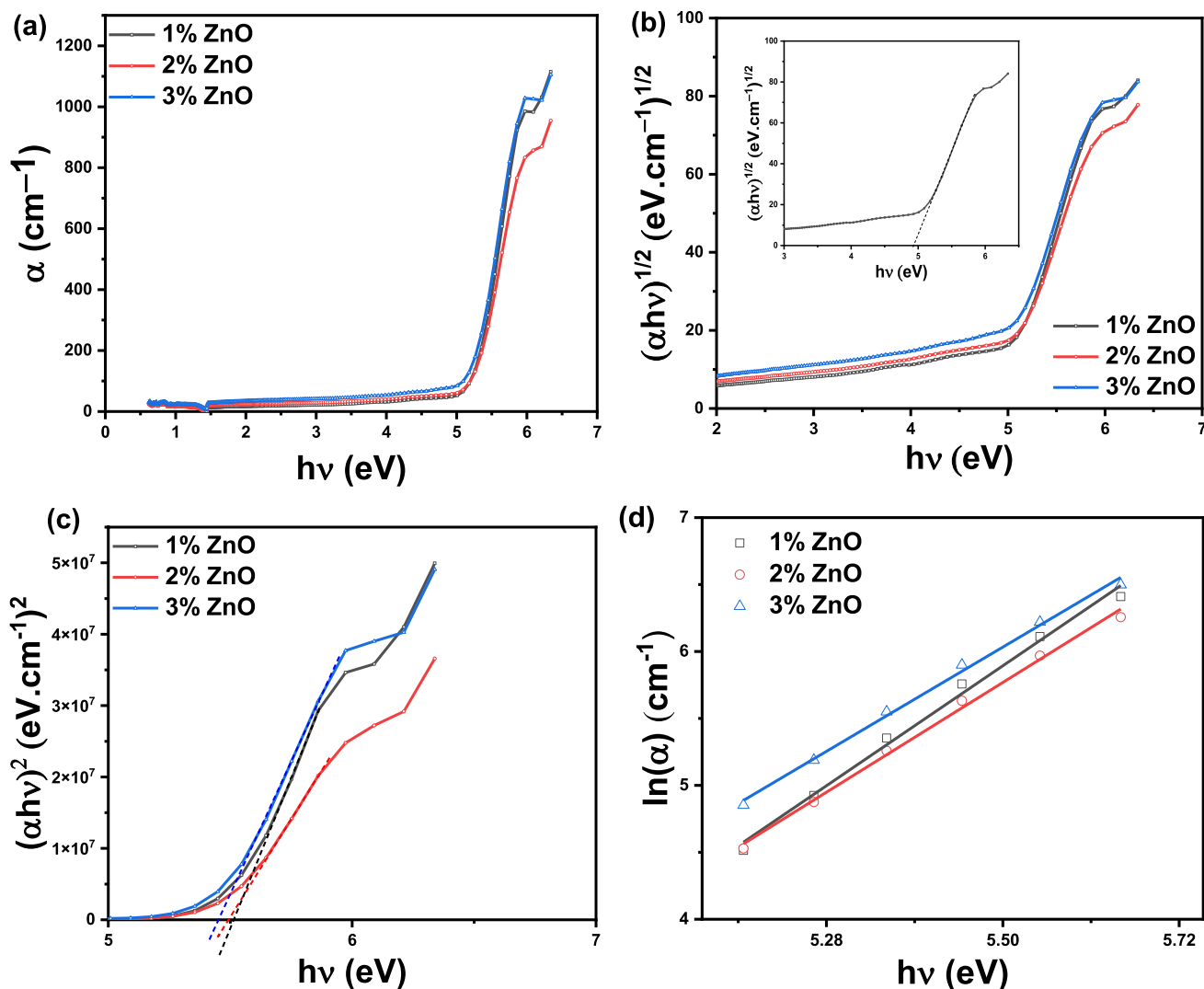


Fig. 3 a The absorption coefficient (α), b $(\alpha h\nu)^{1/2}$, c $(\alpha h\nu)^2$, and d $\ln(\alpha)$ versus the photon energy ($h\nu$) for PVA-ZnO nanocomposites

Table 2 Optical and dispersion parameters of PVA-ZnO nanocomposites

ZnO ratio (wt%)	E_g^d (eV)	E_g^{ind} (eV)	E_e (eV)	E_o (eV)	E_d (eV)	n_o	ϵ_∞	$N/m^* \times 10^{35}$ ($kg^{-1} m^{-3}$)	λ_o (nm)	$S_o \times 10^{-5}$ (nm^{-2})
1	5.51	4.93	0.25	7.99	10.34	1.51	8.97	1.41	155.17	5.38
2	5.50	4.91	0.27	9.61	10.51	1.45	6.13	0.88	134.56	5.90
3	5.45	4.89	0.28	7.88	11.75	1.58	11.59	1.93	157.96	5.96

is used instead of only pure PVA, the absorbance of PVA is greatly enhanced [14].

According to the previous discussion, doping PVA with ZnO change the optical parameter (T, R, and A) to suit it for various application. Modifying T and R will affect the optical band gap, refractive index, optical sheet resistance, and other optical parameters. In the following discussions,

we will calculate various optical parameters using T and R showing the effect of the ZnO ratio on those parameters.

The absorption coefficient (α), $(\alpha h\nu)^{1/2}$, $(\alpha h\nu)^2$, and $\ln(\alpha)$ versus the photon energy ($h\nu$) for PVA-ZnO nanocomposites is shown in Fig. 3a–d, respectively. The absorption coefficient passes two stages: (1) α slightly increased with increasing $h\nu$ to nearly 3–3.5 eV. (2) For photon energy above 4 eV, α is increased exponentially with increasing

$h\nu$. The calculated α at photon energy equals 4 eV is 31.83, 40.71, and 54.61 cm^{-1} for PVA-1 wt% ZnO, PVA-2 wt% ZnO, and PVA-3 wt% ZnO samples, respectively. Above 5 eV, α shows a dramatic increase in its value. At $h\nu = 6$ eV, the attained value of α is 968.760, 838.370, 1027.16 cm^{-1} for PVA-1 wt% ZnO, PVA-2 wt% ZnO, and PVA-3 wt% ZnO samples, respectively. The trend of the absorbance plots of all PVA-ZnO nanocomposites shows a performance reverse to that of the transmission spectrum. The existence of ZnO leads to an absorption band located at 363 nm which agrees with another study [29]. The mechanism of such ultraviolet absorption could be attributed to the utilization of photon energy to excite electrons from the valence to the conduction band.

The plots shown in Fig. 3b, c, $(\alpha h\nu)^{1/2}$, and $(\alpha h\nu)^2$ versus the photon energy, are follow Tauc relation: $(\alpha h\nu)^r = \text{const.}(h\nu - E_g)$ [47]. The direct optical band gap (E_g^d) and indirect optical band gap (E_g^{ind}) was calculated from the $(\alpha h\nu)^{1/2}$, and $(\alpha h\nu)^2$ plots, respectively, by the intercept of the dashed line with the x-axis (or $h\nu$ -axis) at $(\alpha h\nu)^{1/2} = 0$, and $(\alpha h\nu)^2 = 0$, respectively. From Fig. 3b, the indirect bandgap E_g^{ind} value is 4.93, 4.91, and 4.89 eV for PVA-1 wt% ZnO, PVA-2 wt% ZnO, and PVA-3 wt% ZnO nanocomposite, respectively. Meanwhile, from Fig. 3c, the direct bandgap E_g^d value is 5.51, 5.49, and 5.45 eV for PVA-1 wt% ZnO, PVA-2 wt% ZnO, and PVA-3 wt% ZnO nanocomposite, respectively. The value of the width of localized states (E_e) was calculated from the slope of the fitted lines which is associated with the Urbach equation: $(\alpha = \alpha_0 e^{\frac{h\nu}{E_e}})$ [48]. From Fig. 3d, the E_e value is 0.25, 0.27, and 0.28 eV for PVA-1 wt% ZnO, PVA-2 wt% ZnO, and PVA-3 wt% ZnO nanocomposite, respectively. For a clear comparison, the calculated values of E_g^d , E_g^{ind} , and E_e for the investigated

PVA-ZnO nanocomposite are listed in Table 2. The estimated values of the electronic parameters for the PVA-ZnO nanocomposite well agree with the previous studies [23, 29, 30]. The change in the optical band gap could be attributed to the change in the crystallinity and defect generation by various ZnO concentrations. In the present study, the Urbach energy was slightly decreased with increasing the content of ZnO, which shows an opposite trend compared to the study reported by Kumar et al. [49]. Similar to other studies, the optical band gap gets smaller as the ZnO ratio rises, however, the electron transfer across the band gap in the present study can happen either directly or indirectly. Additionally, for all examined nanocomposites, the optical band gap value for direct transition is larger than that for indirect optical band gap.

The increase of the absorption coefficient with increasing the photon energy could be ascribed to the electronic transition from the bonding molecular orbit to the nonbonding molecular orbit. It was observed from the estimated optical bandgap that the incorporation of ZnO nanofiller is like the doping with various metal and metal oxides such as Ni^{2+} and Fe, and significantly affects the optical bandgap of the composite polymer [13, 15]. This observation could be a confirmation of the role of the ZnO fillers inside the host PVA in the improvement of their optical properties. The distinction of the computed values of the optical band gap reflects the role of a configuration of ZnO in altering the electronic structure of the PVA matrix. This diminution due to the induction of new levels in the bandgap leads up to simplifying the transit of electrons from the valence band into these topical levels to the conduction band, consequently the conductivity increment and the bandgap diminution.

Optical density (OD) as a function of the wavelength (λ) for various PVA-ZnO nanocomposites is shown in Fig. 4. The OD is calculated from: $OD = -\log_{10}(T) = 0.434\alpha d$, which represents the dependence of OD on the film thickness d (cm) and α . The value of OD passes two distinct stages: (1) in the wavelength range 200–300 nm values of OD are dramatically decreased with increasing the incident wavelength. (2) Above 300 nm, OD values reach a steady value for the remaining part of the investigated wavelength. At $\lambda = 800$ nm, the steady OD value for PVA-1 wt% ZnO, PVA-2 wt% ZnO, and PVA-3 wt% ZnO nanocomposite is 0.046, 0.074, and 0.099, respectively. Comparing A and OD curves, both A and OD have similar behavior with the wavelength and exhibit a step-change at the same wavelength equal to 867 nm which is equivalent to an energy equal to 1.43 eV.

The evaluation of the refractive index (n) and hence the extension coefficient (k_{ex}) of optical material could be essential as it is widely concerning to the electronic polarization of ions and the optical field inside materials and hence the ability to design various optical devices.

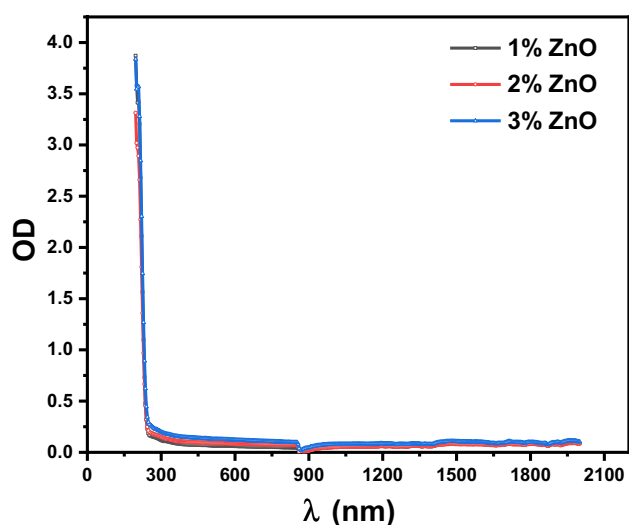


Fig. 4 The optical density (OD) as a function of the incident wavelength (λ) for PVA-ZnO nanocomposites

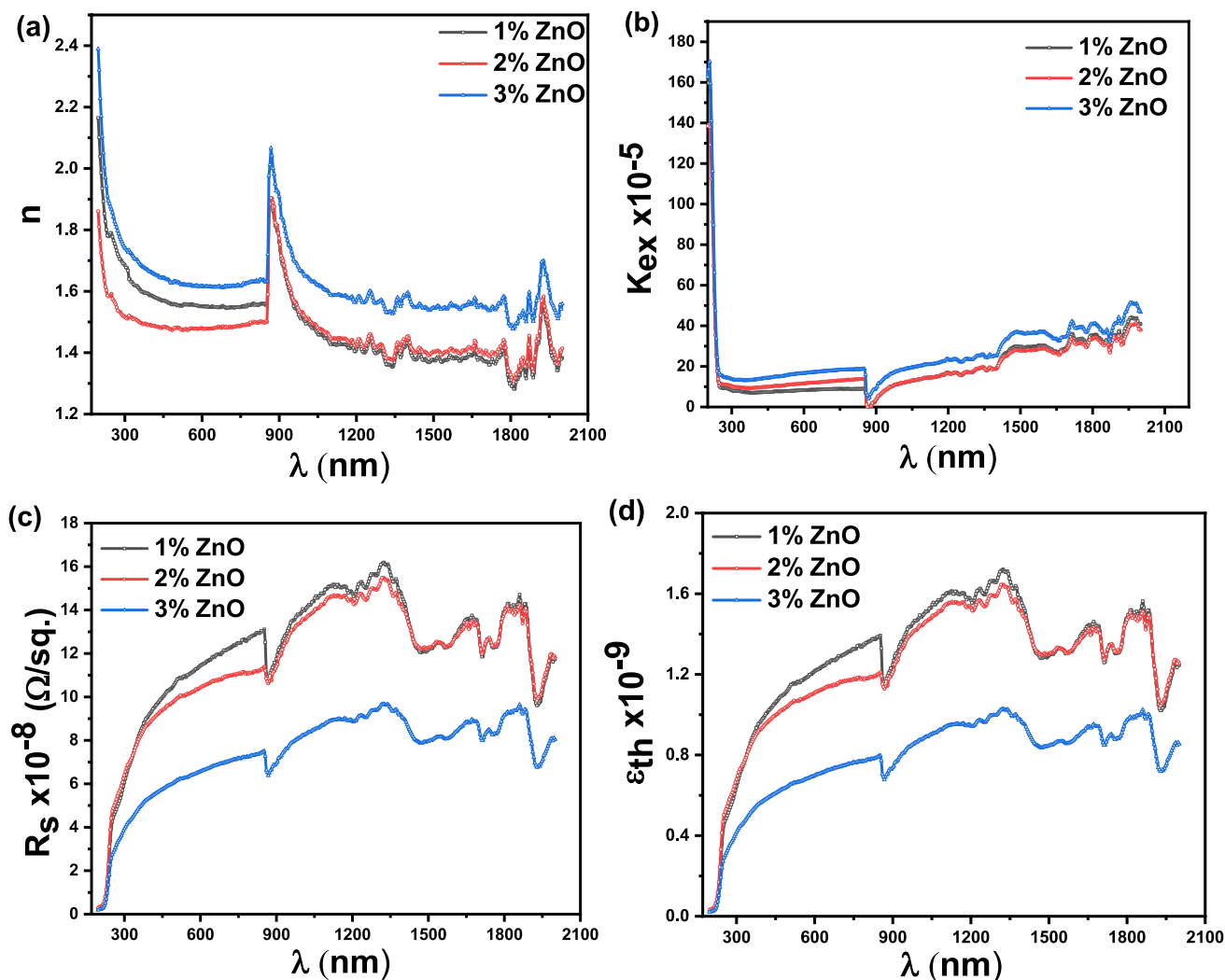


Fig. 5 **a** The refractive index (n), **b** the extension coefficient (k_{ex}), **c** optical surface resistance (R_s), and **d** thermal emissivity (ϵ_{th}) versus the wavelength (λ) for PVA-ZnO nanocomposites

Besides, k_{ex} describes differentiating of the material concerning the light of a given wavelength and shows the absorption differences while the electromagnetic wave propagates through the optical material. The refractive index and the extension coefficient versus the wavelength for PVA-ZnO nanocomposites are shown in Fig. 5a, b, respectively. The value of k_{ex} was calculated from: $k_{ex} = \frac{\alpha\lambda}{4\pi}$ and by substituting k_{ex} into: $n = \sqrt{\frac{4R}{(R-1)^2} - k_{ex}^2} + \frac{R+1}{R-1}$, the refractive index can be calculated [47]. Similarly, k_{ex} and n exhibit the same behavior as A and OD. Both of them decrease significantly with increasing the wavelength in the range 200–300 nm, then pass a steady value in the wavelength range 300–870 nm. However, the main differences in their behavior are that n slightly increase and k_{ex} slightly decreases with increasing the wavelength in the range 870–900 nm, and above 900 nm n slightly decrease

and k_{ex} slightly increase again for the remaining part of the investigated wavelength. The average range of k_{ex} is $0-173 \times 10^{-5}$ for PVA-1 wt% ZnO nanocomposites, this range will be decreased for PVA-2 wt% ZnO nanocomposites, and PVA-3 wt% ZnO nanocomposites, meanwhile increased again for PVA-1 wt% ZnO nanocomposites. For the refractive index, its average range is 1.37 and 1.65. The maximum value of n was observed to be 1.87, 1.9, and 2.06 for PVA-1 wt% ZnO, PVA-2 wt% ZnO, and PVA-3 wt% ZnO nanocomposite, respectively.

The optical surface resistance (R_s) versus the wavelength (λ) for PVA-ZnO nanocomposites is shown in Fig. 5c. The values of R_s are calculated from: $R_s = -\frac{4\pi}{c} \times \frac{1}{n \times \ln(T)}$, where c is the speed of light [50]. The values of R_s pass three stages: (1) in the wavelength range 200–450 nm, the R_s values are significantly increased with

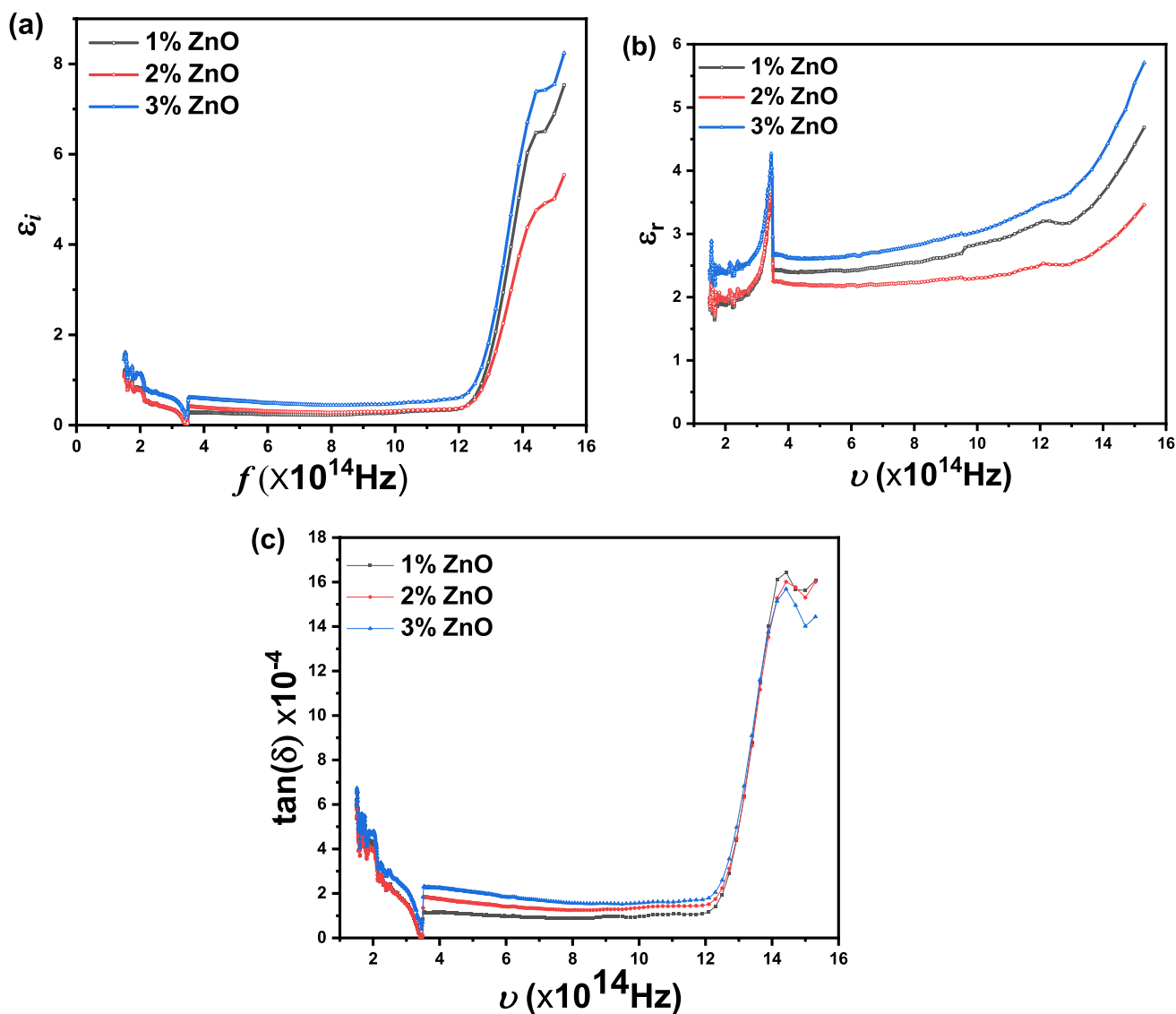


Fig. 6 **a** The imaginary part of the dielectric constant (ϵ_i), **b** the real part of the dielectric constant (ϵ_r), and **c** the loss factor ($\tan(\delta)$) versus the frequency (ν) for PVA-ZnO nanocomposites

increasing the incident wavelength, (2) in the wavelength range 450–850 nm the R_s reach a steady value, and (3) the R_s values oscillated for the remaining part of the investigated wavelength. The value of thermal emissivity (ϵ_{th}) is calculated from: $\epsilon_{th} = 1 - \frac{1}{[1 + (2\epsilon_0 c \times R_s)]^2}$ [51], for PVA-ZnO nanocomposite. From R_s and ϵ_{th} curves, the thermal emissivity curve has a similar trend to the optical surface resistance along the investigated wavelength as shown in Fig. 5d.

The dielectric constants of a material are described by the change in both the real and imaginary parts. The dielectric constant components are significant for the calculation of various optical parameters, the imaginary (ϵ_i) and real (ϵ_r) parts of the dielectric constant versus the incident photon

frequency (ν) for PVA-ZnO nanocomposites are shown in Fig. 6a and b, respectively. The value of ϵ_i and ϵ_r can be calculated from: $\epsilon_i = 2nk_{ex}$, and $\epsilon_r = n^2 - k_{ex}^2$, respectively. ϵ_i passes four stages: (1) in the frequency range $1-1.5 \times 10^{17}$ Hz values of ϵ_i is dramatically increased with increasing the incident photon frequency, (2) in the frequency range $3.5 \times 10^{16}-10^{17}$ Hz, ϵ_i values reach a steady value, (3) at 3.45×10^{16} Hz, the ϵ_i is slightly increased again, and 4) above 3.45×10^{16} Hz, ϵ_i slightly decreases from the steady value.

Similarly, ϵ_r passes four stages: (1) in the frequency range $1-1.5 \times 10^{17}$ Hz values of ϵ_r is dramatically increased with increasing the incident photon frequency, (2) in the photon frequency range $3.5 \times 10^{16}-10^{17}$ Hz, ϵ_r values reach a steady value, (3) at 3.46×10^{16} Hz, the ϵ_r is significantly decreased

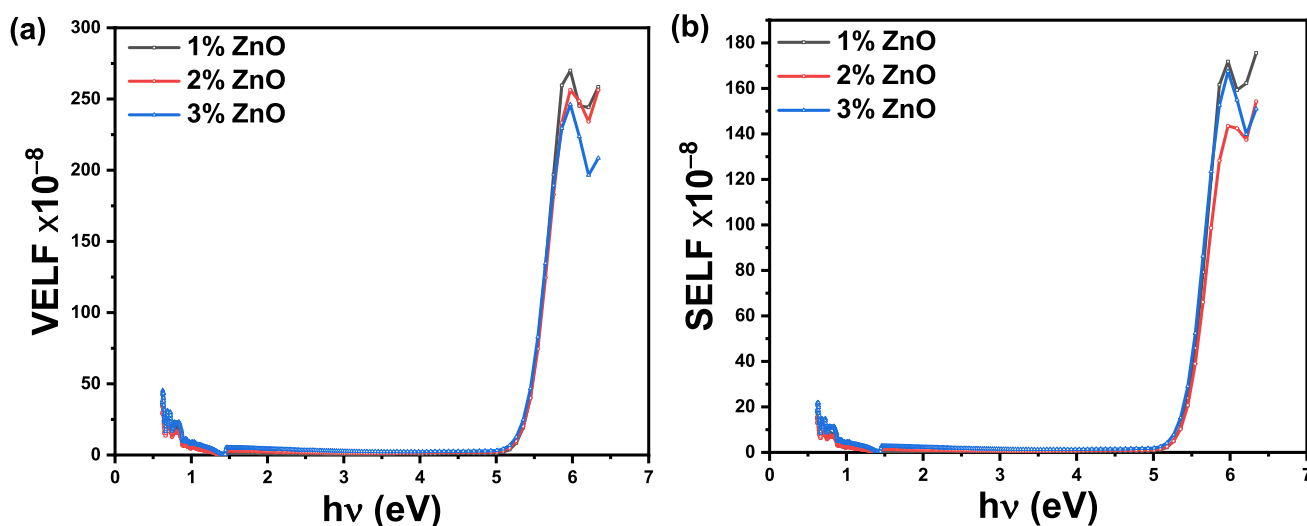


Fig. 7 **a** The volume energy loss (VELF) and **b** surface-energy loss (SELF) versus the photon energy ($h\nu$) for PVA- $x\%$ ZnO nanocomposites

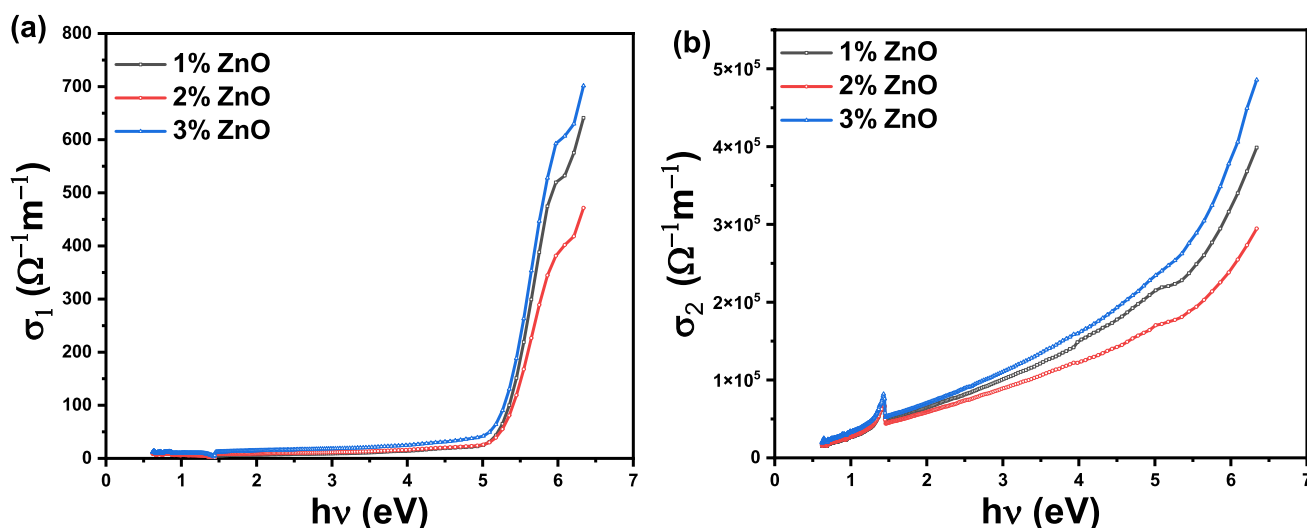


Fig. 8 **a** The optical conductivity (σ_1) and **b** electric conductivity (σ_2) versus the photon energy ($h\nu$) for PVA-ZnO nanocomposites

again with increasing the photon frequency, and (4) above 3.46×10^{16} Hz, the ϵ_r will be decreased again from a steady value. The loss factor, $\tan(\delta)$, versus the photon frequency (ν) for PVA-ZnO nanocomposites is shown in Fig. 6c. The value of loss factor can be estimated from: $\tan(\delta) = \frac{\epsilon_i}{\epsilon_r}$. The change in the dielectric constant components reveals the modification of the chemical composition of the host polymer by the ZnO doping filler.

The energy loss can be presented by two functions called volume energy loss function (VELF), and surface energy loss function (SELF). The VELF presents the energy that is lost by fast electrons inside the bulk material, while the SELF presents the energy loss on the material surface. Both VELF and SELF are a function of the components of the dielectric constants (ϵ_r

and ϵ_i) and can be estimated using: $VELF = \frac{\epsilon_i^2}{\epsilon_r^2 + \epsilon_i^2}$, and $SELF = \frac{\epsilon_i^2}{(\epsilon_r + 1)^2 + \epsilon_i^2}$ [52]. The values of VELF, and SELF gives information about the total energy loss. VELF and SELF versus the photon energy ($h\nu$) for PVA-ZnO nanocomposites are shown in Fig. 7a, b, respectively. The VELF and SELF show the same trend and pass four stages: 1) in the energy range 0.62–1.45 eV, they decrease slightly with increasing energy, (2) in the energy range 1.45–5.3 eV, they reach a steady value, (3) in the energy range 5.3–6 eV, their values are dramatically increased with increasing energy value, (4) above 6 eV, VELF and SELF will show some oscillations.

The complex optical conductivity ($\sigma^* = \sigma_1 + i\sigma_2$) was calculated from the complex dielectric constant ($\epsilon^* = \epsilon_r + i\epsilon_i$)

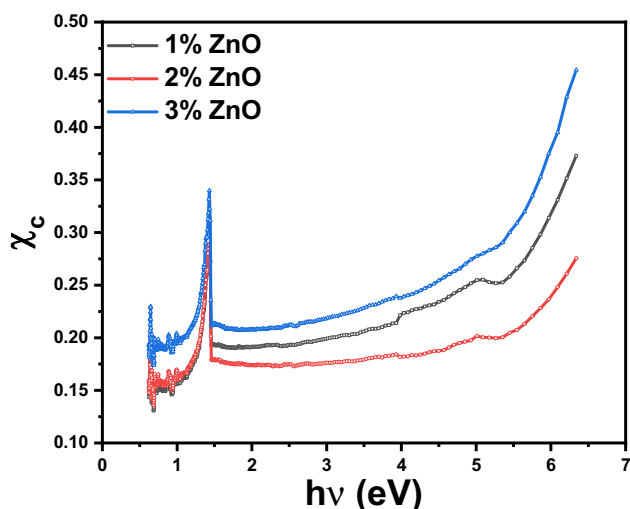


Fig. 9 The electrical susceptibility (χ_c) versus the photon energy ($h\nu$) for PVA-ZnO nanocomposites

and real component σ_1 and imaginary component σ_2 are given from: $\sigma_1 = 4\pi\epsilon_0 \frac{cnk_{ex}}{\lambda}$, and $\sigma_2 = \frac{2\pi c\epsilon_0}{\lambda}(n^2 - k_{ex}^2)$, respectively [53]. The plots of σ_1 and σ_2 versus the photon energy are shown in Fig. 8a, b, respectively, for PVA-ZnO nanocomposites. The values of σ_1 are exponentially increased with increasing the photon energy. The imaginary component, σ_2 , shows a linear increase with increasing the photon energy, $h\nu$, but reveals a small sharp peak at 1.43 eV.

The electrical susceptibility (χ_c) versus the photon energy for PVA-ZnO nanocomposites is shown in Fig. 9, where χ_c is calculated from: $\chi_c = \frac{1}{4\pi}(\epsilon_r - n^2)$. It was observed that χ_c is increased with increasing the photon energy and has one peak at 1.43 eV. The value of χ_c was shifted toward a higher value for PVA-2 wt% ZnO and PVA-3 wt% ZnO nanocomposites.

In the normal dispersion region or so-called transparent region, the dispersion refractive index has been analyzed using the single oscillator model developed by Wemple and DiDomenico [54]. The plot of $(n^2 - 1)^{-1}$ versus $(h\nu)^2$ is shown in Fig. 10a for PVA-ZnO nanocomposite. The value of the average energy of the oscillator (E_o) and the average strength of inter-band optical transitions (E_d) were calculated from the slope and intercept of the fitted data which are estimated from: $(n^2 - 1)^{-1} = \frac{E_o}{E_d} - \frac{(h\nu)^2}{E_o E_d}$ [54]. The numerical values of E_o and E_d for PVA-ZnO nanocomposites are listed in Table 2. By comparing E_o and E_d values for PVA-ZnO nanocomposite, E_o and E_d showed a higher value equal to 9.61 eV and 11.75 eV for PVA-2 wt% ZnO and PVA-3 wt% ZnO, respectively. The value of the static refractive index (n_o) is calculated from: $n_o = \sqrt{1 + \frac{E_d}{E_o}}$, and has an average range started from 1.45 and ended up with 1.58 for PVA-3 wt% ZnO nanocomposite. In the present

work, it was observed that the value of E_o increased with increasing the ZnO content to 2 wt% and then decreased again when the ratio becomes 3 wt%. The observed decrease in E_o could be attributed to the increase in the localized states in the band gap which in turn enhances the low energy transitions leading to a decrease in the value of E_o . It is generally known that dispersion energy is associated with changes in the structural order of the material, which explains the increase in E_d values with increasing ZnO concentration for all PVA-ZnO nanocomposites. From the obtained data we observed that the oscillator energy is related to the average value of the optical band-gap by this deduced empirical equation $E_o = 1.63 \times E_g$ and could be suitable for all PVA-ZnO nanocomposites.

The relation between $(n^2 - 1)^{-1}$ and λ^{-2} is shown in Fig. 10b for PVA-ZnO nanocomposites. The average oscillator strength (S_o) and the average inter-band oscillator wavelength (λ_o) were calculated from the slope and intercept of the fitted data which is estimated from: $(n^2 - 1)^{-1} = \frac{1}{S_o \lambda_o^2} - \frac{1}{S_o} \frac{1}{\lambda^2}$. The estimated values of S_o and λ_o for PVA-ZnO nanocomposites are listed in Table 2. For example, the value of S_o is 5.38×10^{-5} , 5.90×10^{-5} , and $5.96 \times 10^{-5} \text{ nm}^{-2}$, and λ_o values are 155.17, 134.56, and 157.96 nm for PVA-1 wt% ZnO, PVA-2 wt% ZnO, and PVA-3 wt% ZnO nanocomposites, respectively.

The plot n^2 versus λ^2 for PVA-ZnO nanocomposites is shown in Fig. 10c. The plotted points reveal a good fitting to the straight lines that are shown in Fig. 10c and this well agrees with the relation: $n^2 = \epsilon_\infty - \frac{e^2}{4\pi^2 \epsilon_o c^2} \frac{N}{m^*} \lambda^2$ [54]. In this equation, ϵ_∞ , ϵ_o , and c denotes the high-frequency dielectric constant, the vacuum permittivity, and the speed of light, respectively. The maximum value of ϵ_∞ equals 11.59 and was observed for PVA-3 wt% ZnO nanocomposite, meanwhile, the smaller value equals 6.13 and was observed for PVA-2 wt% ZnO nanocomposite. Similarly, the increase of the ZnO ratio to 2 wt% leads to a decrease in free carrier concentration ($\frac{N}{m^*}$) from $1.41 \times 10^{35} \text{ kg}^{-1} \text{ m}^{-3}$ to $8.8 \times 10^{34} \text{ kg}^{-1} \text{ m}^{-3}$ but was increased again to $1.93 \times 10^{35} \text{ kg}^{-1} \text{ m}^{-3}$ for a further increase in ZnO content to 3 wt%. The estimated values of ϵ_∞ and $\frac{N}{m^*}$ for PVA-ZnO nanocomposites are listed in Table 2.

The difference between optical energies for the direct and indirect optical transitions is about 1.4 eV which equals a wavelength of 850 nm. There is a rapid rise or drop (pulse) in the investigated linear and nonlinear optical characteristics at this wavelength or energy value, and the behaviors subsequently resume as before this point with an increase in the photon energy or wavelength. For PVA-based nanocomposites doped with Ni^{2+} at an energy equivalent to the energy difference between the direct and indirect optical band gaps, similar alterations in the optical characteristics were observed [15]. This observation is quite intriguing

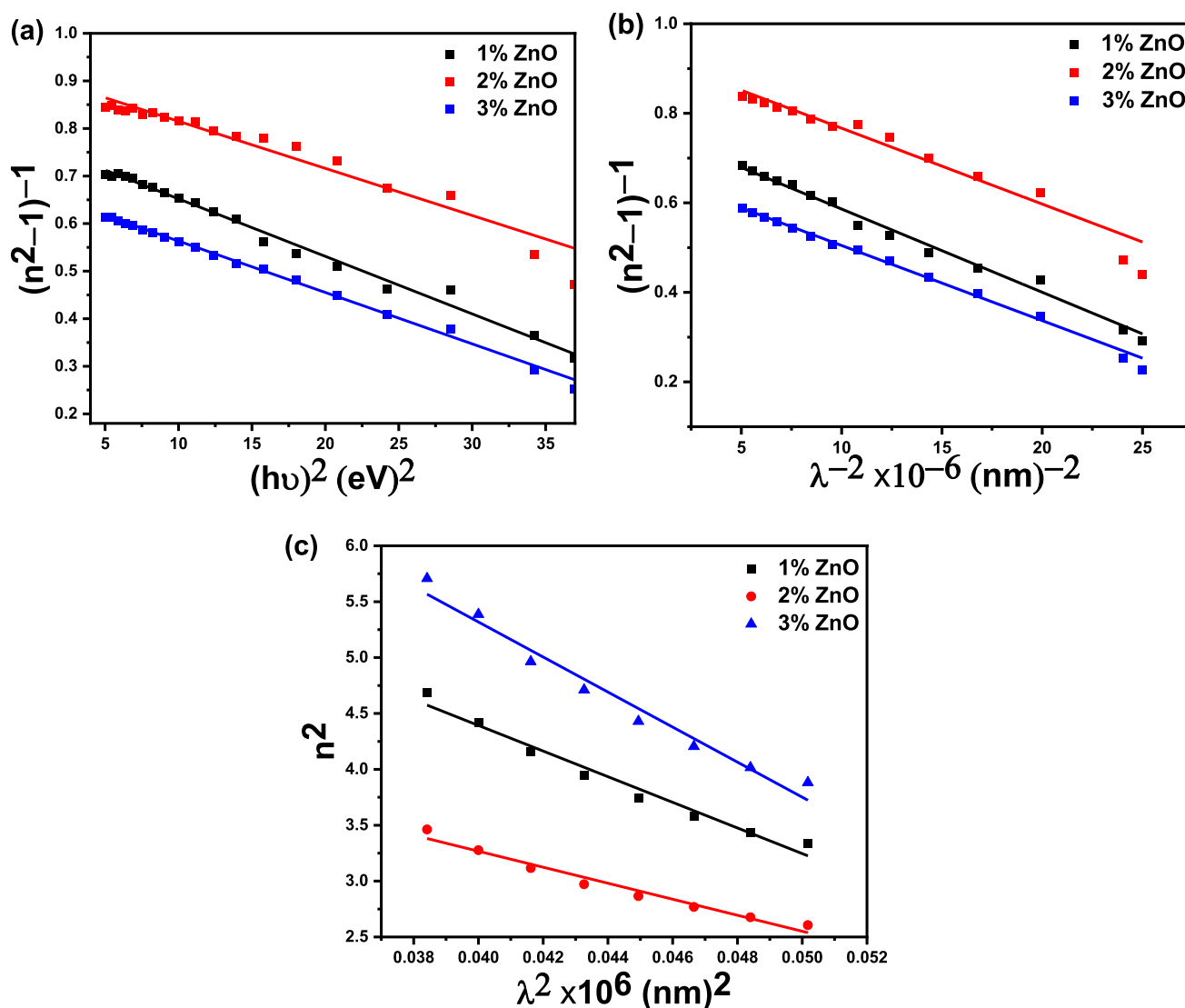


Fig. 10 Plots of **a** $(n^2-1)^{-1}$ versus $(h\nu)^2$, **b** $(n^2-1)^{-1}$ versus λ^{-2} and **c** n^2 versus λ^2 for PVA-ZnO nanocomposites

and has the following justification: the electrons in the confined state and the nearby conduction band electrons are transported to the conduction band when the photon energy reaches 1.4 eV. Consequently, when the energy is equal to or higher than the indirect or direct optical band gap or equal to the difference between them, the optical characteristics will change once again.

Polymer nanocomposites with inorganic/metallic filler components such as ZnO, V₂O₅, graphene, silver (Ag), GaO, MgO, and others have long sparked the interest of scientific and industrial institutions [40, 55–60]. ZnO is an appealing material for photonic applications in the UV or blue spectral areas due to its broad bandgap (3.37 eV), and its high exciton-binding energy allows for effective excitonic emission even at ambient temperature. As a result, they are widely regarded as the most promising candidates for

optoelectronics, sensors, transistors, piezoelectrics, UV-detectors, optical interconnect, UV laser diodes, solar cells, light-emitting diodes (LEDs), photovoltaics, varistors, and other high-power electronics [1, 61].

4 Conclusion

PVA with x wt% ZnO NP dopant (where $x = 1, 2,$ and 3) was produced using the solvent casting method. The synthesized PVA-ZnO hybrid nanocomposites composed of wurtzite hexagonal ZnO phase inside the monoclinic PVA matrix. The structural properties are somewhat influenced by the ZnO ratio; for instance, the size of the crystallites in each phase rose as the ZnO ratio increased. The formation of the Zn–O bond and the functional groups of PVA was

shown, and molecular vibrations inside the nanocomposites were detected. PVA nevertheless exhibited high optical transparency of 65% (low absorption) while containing 3 wt% ZnO NPs. The electron transition via the band gap follows both direct and indirect mechanisms. The difference between the direct and indirect optical band gaps is represented by a pulse shift in the linear and nonlinear parameters. The optical band gap becomes narrower when ZnO is incorporated. The optical conductivity of the PVA material is improved by the doping of 3 wt% of ZnO NPs, which encourages increasing ZnO NP levels in PVA. The majority of the optical characteristics remain steady as the incident photon wavelength shifts beyond 300 nm. The substantial absorption in this range might explain the large shift in optical properties before 300 nm. Our findings indicate that metal oxide such as ZnO NPs doping is a viable approach for regulating and improving the physical characteristics of PVA, particularly its optical properties. The PVA-ZnO nanocomposites' inferred optical and dispersion properties show that they may be used for a variety of optoelectronic applications that call for a broadband gap.

Author Contributions AMA-E: Data curation; methodology; writing the original draft. MR: Investigation; methodology; writing the original draft. TAH: Investigation, Formal analysis; resources, writing the original draft. NMS: Data curation; formal analysis; investigation, writing the original draft. All authors have read and agreed to the published version of the manuscript.

Funding Open access funding provided by The Science, Technology & Innovation Funding Authority (STDF) in cooperation with The Egyptian Knowledge Bank (EKB). The authors have not disclosed any funding.

Data Availability Not applicable.

Declarations

Conflict of interest The authors have not disclosed any competing interests.

Ethical Approval Not applicable.

Open Access This article is licensed under a Creative Commons Attribution 4.0 International License, which permits use, sharing, adaptation, distribution and reproduction in any medium or format, as long as you give appropriate credit to the original author(s) and the source, provide a link to the Creative Commons licence, and indicate if changes were made. The images or other third party material in this article are included in the article's Creative Commons licence, unless indicated otherwise in a credit line to the material. If material is not included in the article's Creative Commons licence and your intended use is not permitted by statutory regulation or exceeds the permitted use, you will need to obtain permission directly from the copyright holder. To view a copy of this licence, visit <http://creativecommons.org/licenses/by/4.0/>.

References

1. A. Gamal El-Shamy, The optical anatomy of new polyvinyl alcohol/zinc peroxide (PVA/ZnO₂) nanocomposite films for promising optical limiting applications. *Progress Org. Coat.* **150**, 105981 (2021)
2. M. Abdolrahimi, M. Seifi, M.H. Ramezanzadeh, Study the effect of acetic acid on structural, optical and mechanical properties of PVA/chitosan/MWCNT films. *Chin. J. Phys.* **56**(1), 221–230 (2018)
3. M. Aslam, M.A. Kalyar, Z.A. Raza, Polyvinyl alcohol: a review of research status and use of polyvinyl alcohol based nanocomposites. *Polym. Eng. Sci.* **58**(12), 2119–2132 (2018)
4. J. Selvi, V. Parthasarathy, S. Mahalakshmi, R. Anbarasan, M.O. Daramola, P.S. Kumar, Optical, electrical, mechanical, and thermal properties and non-isothermal decomposition behavior of poly (vinyl alcohol)–ZnO nanocomposites. *Iran. Polym. J.* **29**, 411–422 (2020)
5. M. Rashad, Tuning optical properties of polyvinyl alcohol doped with different metal oxide nanoparticles. *Opt. Mater.* **105**, 109857 (2020)
6. M. Gökçen, E. Orhan, S. Taran, High photo-responsivity Au/polyvinyl alcohol (PVA)+ di [1-(2-ethoxyethyl)-5-nitrobenzimidazole] copper dichloride/n-Si UV photodiode. *Sens. Actuators A* **315**, 112335 (2020)
7. S. Asadpour, A. Raeisi, M. Kooravand, A. Asfaram, A review on zinc oxide/poly (vinyl alcohol) nanocomposites: synthesis, characterization and applications. *J. Clean. Prod.* **362**, 132297 (2022). <https://doi.org/10.1016/j.jclepro.2022.132297>
8. H.S. Mansur, R.L. Oréfice, A.A.P. Mansur, Characterization of poly (vinyl alcohol)/poly (ethylene glycol) hydrogels and PVA-derived hybrids by small-angle X-ray scattering and FTIR spectroscopy. *Polymer* **45**(21), 7193–7202 (2004)
9. V. Siva, D. Vanitha, A. Murugan, A. Shameem, S. Asath Bahadur, Studies on structural and dielectric behaviour of PVA/PVP/SnO nanocomposites. *Compos. Commun.* **23**, 100597 (2021)
10. A.N. Gheymasi, Y. Rajabi, E.N. Zare, Nonlinear optical properties of poly (aniline-co-pyrrole)@ ZnO-based nanofluid. *Optic. Mater.* **102**, 109835 (2020)
11. S. Dadkhah, Y. Rajabi, E.N. Zare, Thermal lensing effect in laser nanofluids based on poly (aniline-co-ortho phenylenediamine)@ TiO₂ Interaction. *J. Electron. Mater.* **50**(8), 4896–4907 (2021)
12. N.M. Shaalan, T.A. Hanafy, M. Rashad, Dual optical properties of NiO-doped PVA nanocomposite films. *Opt. Mater.* **119**, 111325 (2021)
13. T.S. Soliman, S.A. Vshivkov, Effect of Fe nanoparticles on the structure and optical properties of polyvinyl alcohol nanocomposite films. *J. Non-Cryst. Solids* **519**, 119452 (2019)
14. A. Chebil, B.B. Doudou, C. Dridi, M. Dammak, Synthesis characterization, optical and electrical properties of polyvinyl alcohol/multi-walled carbon nanotube nanocomposites: a composition dependence study. *Mater. Sci. Eng. B* **243**, 125–130 (2019)
15. H.E. Ali, Y. Khairy, Microstructure and optical properties of Ni²⁺-doped PVA for optoelectronic devices. *Physica B* **570**, 41–47 (2019)
16. K.S. Hemalatha, K. Rukmani, N. Suriyamurthy, B.M. Nagabhushana, Synthesis, characterization and optical properties of hybrid PVA–ZnO nanocomposite: a composition dependent study. *Mater. Res. Bull.* **51**, 438–446 (2014)
17. A. Falamas, I. Marica, F. Nekvapil, M. Stefan, G.S. Macavei, L. Barbu-Tudoran, C. Farcau, Surface enhanced fluorescence potential of ZnO nanoparticles and gold decorated ZnO nanostructures embedded in a polyvinyl alcohol matrix. *J. Photochem. Photobiol. A* **438**, 114516 (2023)

18. A. Kayış, M. Kavgacı, H. Yaykaşlı, S. Kerli, H. Eskalen, Investigation of structural, morphological, mechanical, thermal and optical properties of PVA–ZnO nanocomposites. *Glass Phys. Chem.* **47**, 451–461 (2021)
19. A.A. El-Fadl, G.A. Mohamad, A.B. Abd El-Moiz, M. Rashad, Optical constants of Zn_{1-x}LixO films prepared by chemical bath deposition technique. *Physica B* **366**(1–4), 44–54 (2005)
20. M. Rashad, S.A. Al-Ghamdi, A. Obaid, M. Alzahrani, K. Al-Tabaa, S. Al-Osemi, O. Al-Atawi, N. Al-Anzi, S.A.M. Issa, A.M. Abd-Elnaiem, Zinc oxide nanoparticles for adsorption of potassium permanganate from wastewater using shaking method. *Desalination Water Treat* **229**, 227–234 (2021)
21. P. Gopinatha, P. Suresh, V. Jeevanantham, Mechanical, structural and optical properties of pristine and PVA capped zinc oxide nanocomposites. *J. Ovonic Res.* **19**(1), 23 (2023)
22. A. Azmi, K.S. Lau, S.X. Chin, P.S. Khiew, S. Zakaria, C.H. Chia, Zinc oxide-filled polyvinyl alcohol–cellulose nanofibril aerogel nanocomposites for catalytic decomposition of an organic dye in aqueous solution. *Cellulose* **28**, 2241–2253 (2021)
23. K.D. Dejen, E.A. Zereffa, H.C. Ananda Murthy, A. Merga, Synthesis of ZnO and ZnO/PVA nanocomposite using aqueous Moringa oleifera leaf extract template: antibacterial and electrochemical activities. *Rev. Adv. Mater. Sci.* **59**(1), 464–476 (2020)
24. S. Chauhan, A. Kumar, S. Pandit, A. Vempaty, M. Kumar, B.S. Thapa, N. Rai, S.G. Peera, Investigating the performance of a zinc oxide impregnated polyvinyl alcohol-based low-cost cation exchange membrane in microbial fuel cells. *Membranes* **13**(1), 55 (2023)
25. S.S. Mousavi, B. Sajad, M.H. Majlesara, Fast response ZnO/PVA nanocomposite-based photodiodes modified by graphene quantum dots. *Mater. Des.* **162**, 249–255 (2019)
26. M.I. Abd-Elrahman, Synthesis of polyvinyl alcohol–zinc oxide composite by mechanical milling: thermal and infrared studies. *Nanoscale Microscale Thermophys. Eng.* **17**(3), 194–203 (2013)
27. A.F. Mansour, S.F. Mansour, M.A. Abdo, Improvement structural and optical properties of ZnO/PVA nanocomposites. *IOSR J. Appl. Phys.* **7**(2), 60–69 (2015)
28. O. Elkalashy, E. Sheha, Attempt to tune the dielectric and optical properties in PVA/ZnO composite using tetra ethylene glycol dimethyl ether for light emitting devices. *Appl. Phys. A* **124**(8), 549 (2018)
29. T.S. Soliman, A.M. Rashad, I.A. Ali, S.I. Khater, S.I. Elkalashy, Investigation of linear optical parameters and dielectric properties of polyvinyl alcohol/ZnO nanocomposite films. *Physica Status Solidi (a)* **217**(19), 2000321 (2020)
30. A. Muthupandeeswari, P. Kalyani, L.C. Nehru, On the effects of high loading of ZnO nanofiller on the structural, optical, impedance and dielectric features of PVA@ ZnO nanocomposite films. *Polym. Bull.* **78**, 7071–7088 (2021)
31. S. Gupta, A.K. Pramanik, A. Kailath, T. Mishra, A. Guha, S. Nayar, A. Sinha, Composition dependent structural modulations in transparent poly (vinyl alcohol) hydrogels. *Coll. Surf. B* **74**(1), 186–190 (2009)
32. R. Ricciardi, F. Auriemma, C. De Rosa, F. Lauprêtre, X-ray diffraction analysis of poly (vinyl alcohol) hydrogels, obtained by freezing and thawing techniques. *Macromolecules* **37**(5), 1921–1927 (2004)
33. A. Hassen, T. Hanafy, S. El-Sayed, A. Himanshu, Dielectric relaxation and alternating current conductivity of polyvinylidene fluoride doped with lanthanum chloride. *J. Appl. Phys.* **110**(11), 114119 (2011)
34. P. Scherrer, Estimation of the size and internal structure of colloidal particles by means of röntgen. *Nachr. Ges. Wiss. Göttingen* **2**, 96–100 (1918)
35. N.B. Mohamed, M.B. Haj, L. Sellaoui, M. Haouari, H. Ezzaouia, A. Bonilla-Petriciolet, Impact of the stacking fault and surface defects states of colloidal CdSe nanocrystals on the removal of reactive black 5. *Mater. Sci. Eng. B* **265**, 115029 (2021)
36. Z.R. Khan, M.S. Khan, M. Zulfeqar, M.S. Khan, Optical and structural properties of ZnO thin films fabricated by sol-gel method. *Mater. Sci. Appl* **2**(5), 340–345 (2011)
37. T.A. Hamdalla, T.A. Hanafy, A.E. Bekheet, Influence of erbium ions on the optical and structural properties of polyvinyl alcohol. *J. Spectrosc.* (2015). <https://doi.org/10.1155/2015/204867>
38. M. Hamzah, R.M. Ndimba, M. Khenfouch, V.V. Srinivasu, Blue luminescence from hydrothermal ZnO nanorods based PVA nanofibers. *J. Mater. Sci.* **28**, 11915–11920 (2017)
39. J. Naik, R.F. Bhajantri, Impact of ceria nanofillers on temperature dependent electrical and transport properties of PVA solid polymer electrolyte films. *Mater. Res. Express* **5**(6), 065310 (2018)
40. A.M. Abd-Elnaiem, T.A. Hamdalla, S.M. Seleim, T.A. Hanafy, M. Aljohani, M. Rashad, Influence of incorporation of gallium oxide nanoparticles on the structural and optical properties of polyvinyl alcohol polymer. *J. Inorg. Org. Polym. Mater.* **31**(10), 4141–4149 (2021)
41. X.M. Sui, C.L. Shao, Y.C. Liu, White-light emission of polyvinyl alcohol/ZnO hybrid nanofibers prepared by electrospinning. *Appl. Phys. Lett.* **87**(11), 113115 (2005)
42. A. Bera, D. Basak, Effect of surface capping with poly (vinyl alcohol) on the photocarrier relaxation of ZnO nanowires. *ACS Appl. Mater. Interfaces.* **1**(9), 2066–2070 (2009)
43. S.P. Mondal, A. Dhar, S.K. Ray, A.K. Chakraborty, Bonding, vibrational, and electrical characteristics of CdS nanostructures embedded in polyvinyl alcohol matrix. *J. Appl. Phys.* **105**(8), 084309 (2009)
44. E. Rani, R. Aggarwal, A.A. Ingale, K. Bapna, C. Mukherjee, M.K. Singh, P. Tiwari, A.K. Srivastava, Insight into co-operative growth of nearly monodisperse CdS nanocrystals embedded in polyvinyl pyrrolidone. *J. Mater. Sci.* **51**, 1581–1590 (2016)
45. N. Tanaka, K. Ito, H. Kitano, Raman spectroscopic study of hydrogen bonding of poly (N-vinyl-2-pyrrolidone) in heavy water and dimethyl sulfoxide. *Macromol. Chem. Phys.* **195**(10), 3369–3380 (1994)
46. G.D. Mahan, Intrinsic defects in ZnO varistors. *J. Appl. Phys.* **54**(7), 3825–3832 (1983)
47. E.A. Davis, N.F.F. Mott, Conduction in non-crystalline systems V. Conductivity, optical absorption and photoconductivity in amorphous semiconductors. *Philos. Mag.* **22**(179), 0903–0922 (1970)
48. F. Urbach, The long-wavelength edge of photographic sensitivity and of the electronic absorption of solids. *Phys. Rev.* **92**(5), 1324 (1953)
49. N.B. Kumar, V. Crasta, B.M. Praveen, Advancement in microstructural, optical, and mechanical properties of PVA (Mowiol 10–98) doped by ZnO nanoparticles. *Phys. Res. Int.* (2014). <https://doi.org/10.1155/2014/742378>
50. C.C. Wang, Empirical relation between the linear and the third-order nonlinear optical susceptibilities. *Phys. Rev. B* **2**(6), 2045 (1970)
51. M. Reidingner, M. Rydzek, C. Scherdel, M. Arduini-Schuster, J. Manara, Low-emitting transparent coatings based on tin doped indiumoxide applied via a sol–gel routine. *Thin Solid Films* **517**(10), 3096–3099 (2009)
52. M.M. El-Nahass, H.S. Soliman, A.A. Hendi, S. El-Gamdy, Effect of annealing on the structural and optical properties of tetracyanoquinodimethane thin films. *Aust. J. Basic Appl. Sci.* **5**, 145–156 (2011)
53. A. El-Denglawey, V. Sharma, E. Sharma, K.A. Aly, A. Dahshan, P. Sharma, Optical and mechanical properties of Ag doped thermally evaporated SeTe thin films for optoelectronic applications. *J. Phys. Chem. Solids* **159**, 110291 (2021)

54. S.H. Wemple, M. DiDomenico Jr., Behavior of the electronic dielectric constant in covalent and ionic materials. *Phys. Rev. B* **3**(4), 1338 (1971)
55. M. Abdelaziz, M.M. Ghannam, Influence of titanium chloride addition on the optical and dielectric properties of PVA films. *Physica B* **405**(3), 958–964 (2010)
56. A.M.A. Shamekh, N.M. Shaalan, T.A. Hanafy, M. Rashad, Linear/nonlinear optical properties of functional inorganic MgO nanofiller in PVA transparent polymer for flexible optoelectronic devices. *Physica B* **651**, 414617 (2023)
57. J. Li, L. Shao, L. Yuan, Y. Wang, A novel strategy for making poly (vinyl alcohol)/reduced graphite oxide nanocomposites by solvothermal reduction. *Mater. Des. 1980–2015* **54**, 520–525 (2014)
58. I.-C. Yao, T.-Y. Tseng, P. Lin, ZnO nanorods grown on polymer substrates as UV photodetectors. *Sens Actuators A* **178**, 26–31 (2012)
59. X. Gong, C.Y. Tang, L. Pan, Z. Hao, C.P. Tsui, Characterization of poly (vinyl alcohol)(PVA)/ZnO nanocomposites prepared by a one-pot method. *Compos Part B* **60**, 144–149 (2014)
60. D.M. Fernandes, A.A. Winkler Hechenleitner, S.M. Lima, L.H.C. Andrade, A.R.L. Caires, E.A. Gómez, Pineda., Preparation, characterization, and photoluminescence study of PVA/ZnO nanocomposite films. *Mater. Chem. Phys.* **128**(3), 371–376 (2011)
61. V. Viswanath, S.S. Nair, G. Subodh, C.I. Muneera, Zinc oxide encapsulated poly (vinyl alcohol) nanocomposite films as an efficient third-order nonlinear optical material: structure, microstructure, emission and intense low threshold optical limiting properties. *Mater. Res. Bull.* **112**, 281–291 (2019)

Publisher's Note Springer Nature remains neutral with regard to jurisdictional claims in published maps and institutional affiliations.